K-fiber bundles in the mitotic spindle are mechanically reinforced by Kif15

Marcus A Begley[1], April L Solon[2], Elizabeth Mae Davis[1], Michael Grant Sherrill[1], Ryoma Ohi[2], Mary Williard Elting[1,3*]

[1]Department of Physics, North Carolina State University, Raleigh, NC
[2]Department of Cell & Developmental Biology, University of Michigan, Ann Arbor, MI
[3]Quantitative and Computational Developmental Biology Cluster, North Carolina State University, Raleigh, NC
Correspondence: mary.elting@ncsu.edu

Abstract

The mitotic spindle, a self-constructed microtubule-based machine, segregates chromosomes into two eventual daughter nuclei. In mammalian cells, microtubule bundles called kinetochore-fibers (k-fibers) anchor chromosomes to the spindle poles, vitally supporting spindle function. Yet, how they achieve mechanical integrity is not well-understood. We sever k-fibers using laser ablation, testing the contribution that forces at minus-ends make to k-fiber cohesion. We measure the physical response of the remaining kinetochore-bound segments. We observe that microtubules within ablated k-fibers often, but not always, splay apart from their minus-ends. Furthermore, we find that minus-end clustering forces induced in response to ablation seem at least partially responsible for k-fiber splaying. We also investigate the role of the putative k-fiber binding molecule kinesin-12 Kif15. We find that pharmacological inhibition of Kif15 microtubule binding reduces k-fiber mechanical integrity. In contrast, inhibition of its motor activity but not its microtubule binding does not greatly affect splaying. Altogether, the data suggest that forces holding k-fibers together are of similar magnitude to other spindle forces, and that Kif15, acting as a microtubule crosslinker, helps fortify and repair k-fibers.

Introduction

The mammalian mitotic spindle is a microtubule-based machine responsible for accurate chromosome segregation during cell division. In order to perform their essential function, spindles must be both robust and adaptable in the highly dynamic cellular environment. Kinetochore-fibers (k-fibers), microtubule bundles that link centrosomes to chromosomes, must therefore also be both robust and dynamic (McDonald et al. 1992; Hays, Wise, and Salmon 1982). In Ptk2 cells, k-fibers include both kinetochore microtubules and associated non-kinetochore microtubules (Nicklas, Kubai, and Hays 1982; Hays and Salmon 1990; McDonald et al. 1992). Whereas the non-kinetochore microtubules often interdigitate with the fiber at an angle, the kinetochore microtubules, those attached “end-on” to the kinetochore, form

a parallel array of ~25 microtubules that runs from the kinetochore to the pole and defines the fiber's trajectory (McDonald et al. 1992). A number of sharp contrasts exist between the mechanical behaviors of k-fibers and those of individual spindle microtubules. For example, while single microtubules turn over rapidly, k-fibers are more stable and turn over less frequently (McDonald et al. 1992; Zhai, Kronebusch, and Borisy 1995; Mitchison 1989). The turnover of k-fibers contributes to their ability to generate forces that center chromosomes at the spindle midzone and attach chromosomes in an error-free fashion, while also maintaining structural integrity (Hays, Wise, and Salmon 1982; Hays and Salmon 1990; McDonald et al. 1992).

It is not yet clear how interactions between k-fiber microtubules, such as those through microtubule crosslinkers, contribute to the dynamic behavior and/or temporal longevity of the fiber as a whole. While individual microtubules are already quite stiff, with persistence lengths of around 1 mm (van Mameren et al. 2009), k-fiber bundles appear to be much straighter and stiffer than individual microtubules (Goshima, Nédélec, and Vale 2005), suggesting that they do mechanically reinforce each other. Although the stabilization of inter-microtubule bonds and repair of any physical k-fiber damage by microtubule crosslinkers could contribute to the cohesive strength of the fiber, the effects of crosslinking molecules on k-fiber stiffness has yet to be fully determined (Nicklas, Kubai, and Hays 1982; Nixon et al. 2015). A handful of MAPs, such as the kinesin-12 Kif15 (Sturgill et al. 2014) and its regulator Tpx2 (Bird and Hyman 2008; Sturgill et al. 2014; Mann, Balchand, and Wadsworth 2017), the clathrin/chTOG/TACC3 complex (Booth et al. 2011; Nixon et al. 2015; Cheeseman et al. 2013; Royle, Bright, and Lagnado 2005), HURP (Silljé et al. 2006; Tsuchiya et al. 2018), and kinesin Kif18A (Ye et al. 2011; Mayr et al. 2007) have been shown to localize preferentially to k-fibers and/or to stabilize them, thereby promoting efficient and reliable mitotic progression. However, their precise contributions to k-fiber mechanics and force production remain an open question.

The kinesin-12 Kif15 is well-positioned to shape k-fiber mechanics through both passive cross-linking and active force production. Kif15 has been studied in the context of spindle assembly, because it can drive spindle assembly in the absence of Eg5 function (Tanenbaum et al. 2009). Indeed, both kinesins are capable of crosslinking microtubule pairs and sliding antiparallel microtubules apart (Kapitein et al. 2005; Drechsler et al. 2014; Reinemann et al. 2017). Through this mechanism, Kif15 can antagonize inward forces generated by minus-end-directed motors, thereby enforcing spindle bipolarity, and separating centrosomes in cells adapted to grow in the presence of Eg5 inhibitors (Sturgill and Ohi 2013; Raaijmakers et al. 2012). This redundancy between Kif15 and Eg5 is of particular interest as a potential factor in the disappointing ineffectiveness thus far of Eg5 inhibitors as cancer therapeutics (Tanenbaum et al. 2009; Milic et al. 2018; Dumas et al. 2019; Rath and Kozielski 2012). Furthermore, Kif15 upregulation is found in a number of cancer types and can result in rapid cancer cell proliferation (Wang et al. 2017; Zhao et al. 2019; Yu et al. 2019; Qiao et al. 2018; Sun et al. 2020; Terribas et al. 2020; Ma et al. 2014). Under normal circumstances, however, Kif15 localizes predominantly to k-fiber microtubules. Its function on k-fibers is largely unexplored, although it is presumably from this location that the motor slides antiparallel microtubules apart. In addition, some evidence suggests that Kif15 coordinates the movement of neighbor sister kinetochores within the spindle (Vladimirou et al. 2013).

These characteristics of Kif15, especially its temporal and spatial spindle localization, indicate that it might provide some contribution to the mechanical and dynamical properties of k-fibers themselves. The oligomerization state of Kif15 *in vivo* is not yet clear, and it may behave as either a tetramer or a dimer (Drechsler et al. 2014; Mann, Balchand, and Wadsworth 2017; Reinemann et al. 2017). However, it has a second microtubule binding site, in addition to its motor domain, giving it the ability to bundle microtubules even in a dimeric state (Sturgill et al. 2014). Yet, despite this inherent microtubule-binding activity, Kif15 requires its binding partner, Txp2, for recruitment to the spindle (Tanenbaum et al. 2009). Furthermore, *in vitro* data indicate that Tpx2 increases Kif15 microtubule binding while decreasing motor activity (McHugh et al. 2018; Mann, Balchand, and Wadsworth 2017; Drechsler et al. 2014), emphasizing the importance of this interaction for Kif15 k-fiber bundling, and raising the question of how important motor activity is for this function.

To understand the contribution Kif15 may make to the dynamics and structural maintenance of the k-fiber, we examine the function of Kif15 in mitotic mammalian Ptk2 kidney epithelial cells. First, we use laser ablation to create short k-fiber stubs and find that the microtubules of these stubs often splay apart. We examine the effect on this splaying of the poleward transport response, a previously-characterized response in which cells reconnected ablated microtubule minus-ends. Acting in cooperation with NuMA and dynactin, the minus-end-directed motor dynein pulls these minus-ends toward their corresponding pole until they reach the centrosome, resulting in the reformation of a full-length k-fiber and the complete mechanical reconnection of the kinetochore to the centrosome (Khodjakov et al. 2003; Elting et al. 2014). To probe the role of Kif15 in k-fiber integrity, we test the effect of two Kif15 inhibitors (Kif15-IN-1 and GW108X) on k-fiber splaying. Kif15-IN-1 has been suggested to stabilize a microtubule-bound rigor state (Milic et al. 2018), whereas GW108X blocks the attachment of Kif15's motor head to microtubules (Dumas et al. 2019). Ablation experiments in cells treated with GW108X reveal a heightened sensitivity to these minus-end-directed forces. In contrast, we do not observe this effect in cells treated with Kif15-IN-1. Therefore, the data suggest that, independently of its motor activity, Kif15 mechanically reinforces k-fiber structure by binding and crosslinking k-fiber microtubules.

Results and Discussion

K-fiber stubs are dynamically held together along their lengths, by connections that can be disrupted and reformed

We performed laser ablations in metaphase Ptk2 cells expressing GFP-α-tubulin to remove minus-end forces holding k-fibers together and determine the degree to which k-fibers remain cohesive along their lengths. The mechanical response to ablation commonly consisted of two readily observed behaviors, "poleward transport" and "splaying". Easily identifiable poleward transport, a well-documented post-ablation response (Khodjakov et al. 2003; Elting et al. 2014), followed nearly all ablations. The second frequently seen post-ablation behavior, which we term "splaying", is the dissociation of the k-fiber stub's microtubules along its length. While microtubule plus ends remain intact at the kinetochore, the minus ends of k-fiber stub

microtubules come apart, losing the tightly-cohesive appearance typically associated with k-fibers (Figure 1A; Supplemental Video SV1). While the vast majority of k-fiber stubs are physically reincorporated into the spindle as it repairs itself, regardless of whether or not the stub ever splays (Figure 1, B and C; Supplemental Figure S1F; Supplemental Video SV1, SV2), k-fiber stub splaying occurs following about half of all ablations, suggesting both that the forces that bind neighboring k-fiber microtubules along their lengths can be overcome and broken during spindle repair and that the strength of these crosslinking bonds is inline with the strength of other mitotic spindle forces (Figure 1D).

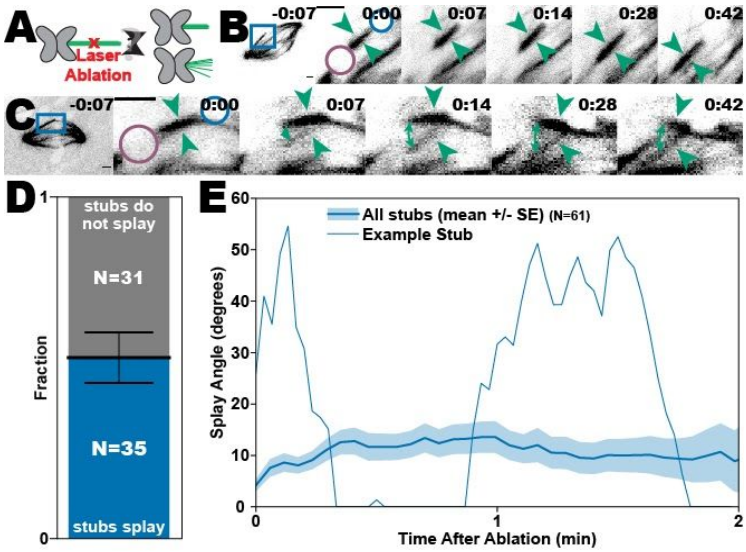

Figure 1: Ablated k-fiber stubs often splay apart. (A) Schematic of k-fiber ablation experiment. Following ablation (red 'X'), k-fiber stubs demonstrate either "no splaying" (top) or "splaying" (bottom). (B&C) Typical examples of k-fiber stubs in Ptk2 cells, expressing GFP-α-tubulin, that do not splay (B) and that do splay (C). The ablation spot (magenta circle), k-fiber stub (green arrows), and chromosomes (blue circle) are labeled in the first post-ablation frame for both k-fiber stubs. All scale bars are 2 μm and timestamps are in min:sec. (D) Roughly half of ablated k-fiber stubs splay at some point during spindle repair. Error bar indicates the square root of the number of splayed events, as an estimate on the variation in this number assuming Poisson statistics. (E) Example trace (narrow blue line) showing the angle over time of a single ablated k-fiber stub, and the average (bold blue line) angle of all stubs. Although the average splay angle gradually increases to about 13°, before gradually decreasing, splaying varies widely among individual k-fiber stubs, with many splaying and "zipping up" multiple times and at different points during repair. Shaded region represents average +/- standard error on the mean.

Although splaying is most commonly observed as the apparent separation into only two microtubule bundles (Figure 2D), the timing, duration, and repetition of these splaying events is highly variable among individual k-fiber stubs. For instance, some time after a k-fiber stub splays, the splayed microtubule bundles will "zip up", reforming into a single tightly-bound k-fiber, a process that usually occurs simultaneously, all along the k-fiber stub's length. While this connection visually appears complete, it is often not final, as many k-fiber stubs undergo multiple splay-zip cycles during spindle repair (Figure 1E). Therefore, even though the collective average splay angle provides valuable insight into the overall magnitude and timescale of k-fiber stub splaying, it is important to note that aggregate metrics such as this obscure the significant temporal variability of splay-zip behavior among individual k-fiber stubs (Figure 1E).

Minus-end-directed forces can pry apart ablated k-fibers

Nearly all k-fiber stubs that splayed did so after the initiation of poleward transport (Figure 2A). Furthermore, the maintenance of lateral inter-microtubule connections within k-fiber stubs

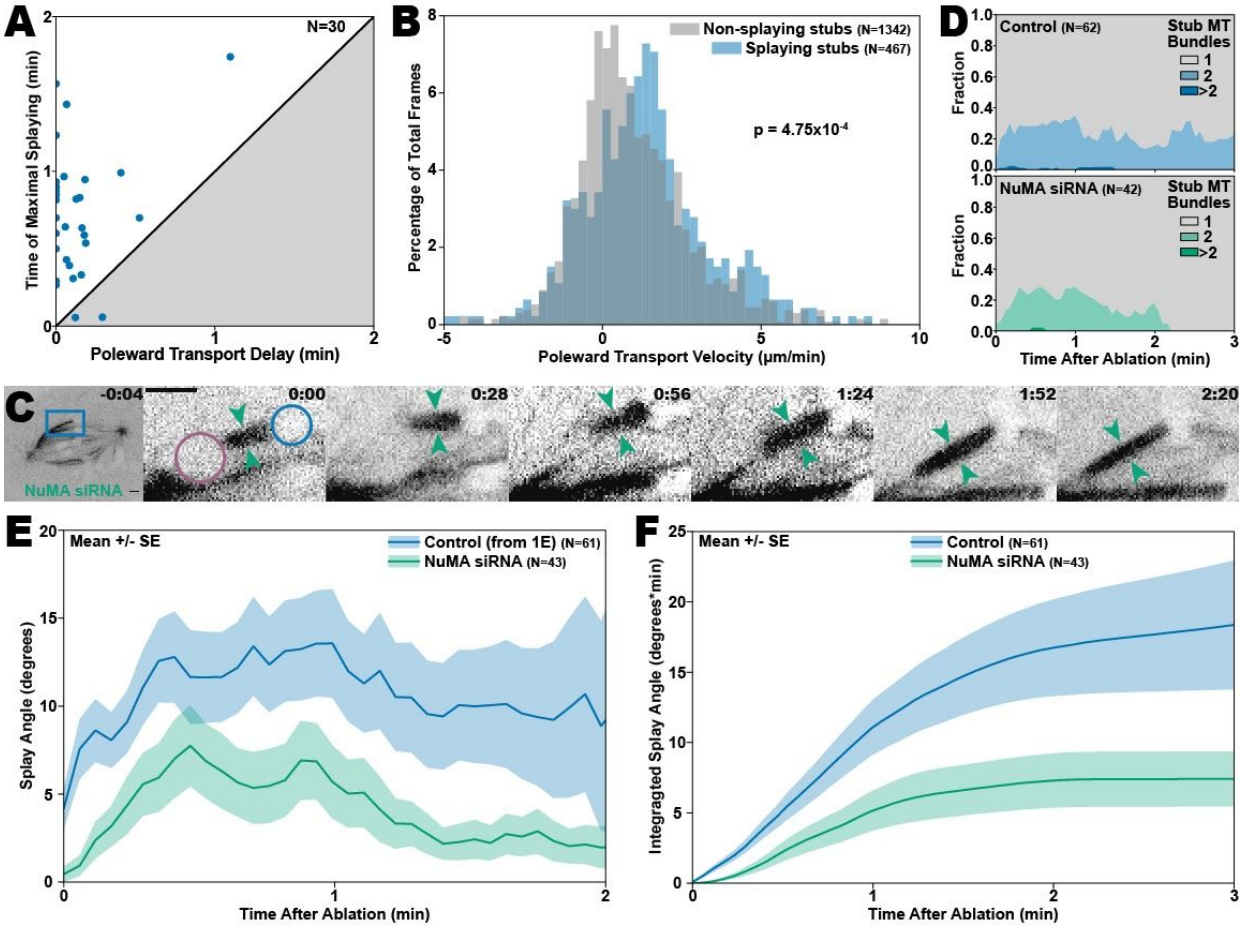

Figure 2: Forces from poleward transport of ablated k-fiber stubs increase the degree of splaying. (A) Maximal splaying typically occurs after the onset of poleward transport for untreated k-fiber stubs. Points represent individual k-fiber stubs. (B) K-fiber stubs undergoing rapid poleward transport are more likely to splay. Here the x-axis is the instantaneous poleward transport velocity and the y-axis is the percentage of time points in each histogram bin. (C) Example of an ablated k-fiber stub in a spindle of a Ptk2 cell expressing GFP-α-tubulin treated with NuMA siRNA. Following ablation, the k-fiber stub is transported poleward without splaying. The ablation spot (magenta circle), k-fiber stub (green arrows), and chromosomes (blue circle) are labeled in the first post-ablation frame. All scale bars are 2 µm and timestamps are in min:sec. (D) K-fiber stubs in spindles treated with NuMA siRNA (bottom, green) splay later than k-fiber stubs from control cells (top, blue) and do not stay splayed for as long. The y-axis represents the fraction of k-fiber stubs at each timepoint, consisting of 1, 2, or more than 2 visibly distinguishable microtubule bundles. (E) NuMA siRNA reduces splaying, compared with untreated cells. Shaded regions represent average +/- standard error on the mean. Note: these data for control k-fiber stubs were also shown in Fig. 1E, above. (F) Total splaying, measured as the integration of data shown in (E), is lower in cells treated with NuMA siRNA. Shaded regions represent average +/- standard error on the mean.

seemed somewhat velocity-dependent, as k-fiber stubs experiencing a greater poleward velocity in a given moment were more likely to be splayed than more slowly transported stubs (Figure 2B). These data suggest that poleward transport can itself promote splaying, with

increasing probability of splaying for k-fiber stubs experiencing stronger poleward-directed forces.

Nuclear mitotic apparatus protein (NuMA) has been shown to be required for rapid and robust poleward transport of loose spindle microtubule minus ends, ensuring the maintenance of spindle poles (Elting et al. 2014; Khodjakov et al. 2003). NuMA is recruited to these minus ends when they appear and in turn recruits cytoplasmic dynein and dynactin (Hueschen et al. 2017), coalescing NuMA/dynein/dynactin complexes to the ablated k-fiber stub minus-end. Dynein motors, which are minus-end-directed, bind to another spindle microtubule and exert minus-end-directed force on the NuMA-bound microtubule, thereby transporting the k-fiber stub poleward as its cargo (Elting et al. 2014; Khodjakov et al. 2003). Because of this known mitotic function of the NuMA/dynein/dynactin complex and the apparent dependence of k-fiber stub splaying on poleward transport, we next investigated the potential role of NuMA in splaying. Specifically, we depleted NuMA via siRNA and then performed the same ablation experiments as before in these NuMA knockdown spindles (Figure 2C). As expected, poleward transport begins later and is more gradual for ablated k-fiber stubs in NuMA siRNA cells compared to those in control cells (Supplemental Figure S1D).

Based on NuMA's established role as a mitotic spindle crosslinker, as well as its k-fiber localicalization (Gaglio et al. 1996; Elting et al. 2017; Supplemental Figure S1A), we initially hypothesized that NuMA might contribute to crosslinking within the k-fiber by mechanically bridging neighbor k-fiber microtubules. Strikingly, we instead observed that splaying of ablated k-fiber stubs is much more gradual initially and reduced throughout spindle repair when NuMA is depleted (Figure 2D-F). Thus, it seems that the NuMA/dynein/dynactin complex, functioning as a minus-end-directed force generator, primarily works to instead pry ablated k-fiber stubs apart. We hypothesize that this occurs when some of the multiple dynein motors within the detected minus-end bind to different track microtubules that are not precisely parallel. These data reinforce the hypothesis that minus-end-directed forces involved in poleward transport, such as those exerted by NuMA/dynein/dynactin, contribute to the frequent longitudinal dissociation of k-fiber microtubules from each other.

Kif15 binds and crosslinks k-fiber microtubules to promote k-fiber cohesion

We next tested for any potential roles in k-fiber cohesion of Eg5 or Kif15, both plus-end-directed crosslinking motors, via pharmacological inhibition. Based on the delayed poleward transport and reduced splaying of k-fiber stubs with NuMA depletion, as well as the fact that poleward transport has been shown to be slightly faster with Eg5 inhibition (Elting et al. 2014), one would expect that the poleward transport and, therefore, the splaying behaviors of ablated k-fiber stubs would remain unchanged (or potentially even increase) with the inhibition of Eg5. Indeed, both the poleward transport and splaying of ablated k-fiber stubs in STLC-treated spindles are generally similar to that of k-fiber stubs in untreated spindles (Supplemental Figure S1, D-F).

On the other hand, pharmacological inhibition of Kif15 revealed a more specific role in k-fiber mechanics. For these experiments, we used two Kif15 inhibitors that act by different mechanisms. Kif15-IN-1 arrests the motor in a microtubule-bound state, and thus blocks motility without disrupting its ability to crosslink microtubules (Milic et al. 2018). By contrast, GW108X

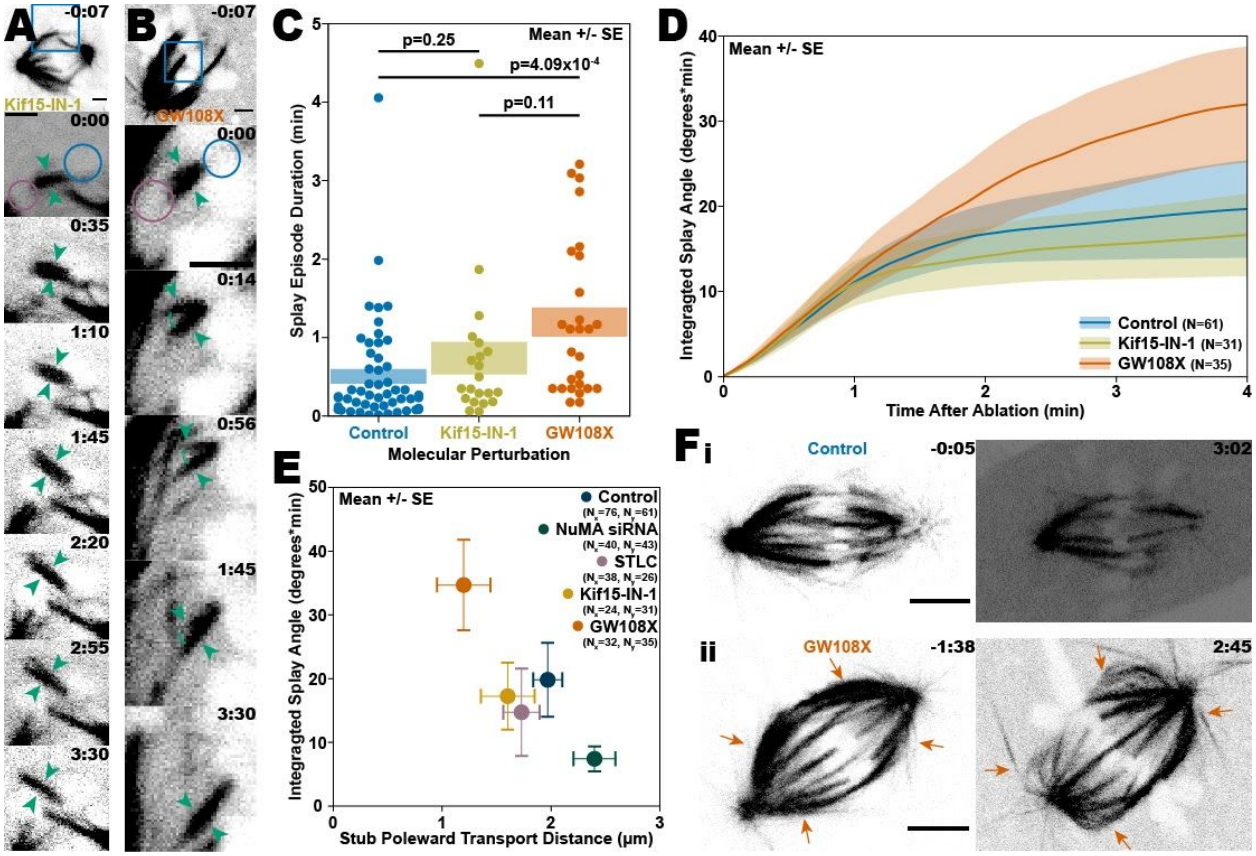

Figure 3: Crosslinking from Kif15 mediates the mechanical integrity of the k-fiber. (A & B) Typical examples of behavior of ablated k-fibers in spindles of Ptk2 cells treated with Kif15 inhibitors. The poleward transport of k-fiber stubs from Ptk2 cells treated with Kif15-IN-1 (A) is occasionally drastically delayed or entirely absent, and, in GW018X-treated cells (B), many of these k-fiber stubs that are not reincorporated into the spindle nonetheless splay. The ablation spot (magenta circle), k-fiber stub (green arrows), and chromosomes (blue circle) are labeled in the first post-ablation frame of each panel. All scale bars are 2 μm and timestamps are in min:sec. (C) Kif15 inhibition by GW108X prolongs splaying. The y-axis is the length of time between when a k-fiber stub begins splaying and when the k-fiber stub is "zipped up". Shaded regions represent average +/- standard error on the mean and numbers at the top of the plot represent p-values. (D) Total splaying, measured as the integration of k-fiber stub splay angle over time, is greater for k-fiber stubs in cells treated with GW108X (which inhibits crosslinking) but is about the same for k-fiber stubs in cells treated with KIF15-IN-1 (which solely inhibits motor activity), when compared to control k-fiber stubs. Shaded regions represent average +/- standard error on the mean. (E) Although treatment with GW108X reduces the poleward transport of ablated k-fiber stubs, relative to k-fiber stubs in untreated cells, these stubs still exhibit greater total splaying. In contrast, treatment with KIF15-IN-1 does not alter the total amount of splaying. Whiskers represent average +/- standard error on the mean. (F) Unablated k-fibers in control spindles usually remain tightly bound throughout metaphase in control spindles (i), while outer k-fibers (arrows) in spindles from GW108X-treated cells (ii) sometimes buckle and splay, while still attached at both the pole and kinetochore. Scale bars are 5 μm and timestamps are in min:sec.

prevents the motor domain of Kif15 from binding the microtubule track, thus preventing the formation of microtubule crosslinks (Dumas et al. 2019).

Unexpectedly, the two Kif15 inhibitors, both of which cause loss of motor function, significantly perturb spindle repair, as shown by poleward transport that is more delayed than in control spindles, and in the case of GW108X, is even more delayed than in NuMA siRNA spindles (Figure 3, A and B; Supplemental Figure S1E). Under both Kif15 inhibition conditions, the spindle occasionally fails to repair altogether during observation, leaving the k-fiber still unattached to the pole at the end of filming (Supplemental Figure S1F). Although poleward transport of severed microtubule minus-ends has been strongly coupled with minus-end-directed force production by dynein (Elting et al. 2014; Khodjakov et al. 2003; Hueschen et al. 2017), a few mechanisms might help explain the apparent additional requirement for Kif15, a plus-end-directed motor, in efficient poleward transport. For instance, Kif15 may act on anti-parallel overlaps near the middle of the spindle to help transport k-fiber stubs poleward following ablation. Alternatively, Kif15-mediated crosslinking might help mechanically anchor track microtubules on which the NuMA/dynein complex walks when transporting ablated k-fiber stubs. Finally, it is also possible that effective poleward transport of ablated k-fibers requires normal k-fiber architecture, which may be disrupted when Kif15 is inhibited (see below). Further investigation will be needed to discern the role of Kif15 in minus-end-directed force generation and the mechanism by which this force is produced.

Since Kif15 inhibition seems to slow and delay poleward transport of ablated k-fiber stubs, one would expect some reduction of splaying when compared with k-fiber stubs in control spindles, as we saw in the NuMA depletion experiments. Instead, stub splaying in cells treated with Kif15-IN-1 occurs with roughly the same frequency, duration, and magnitude as in untreated cells, while GW108X treatment seems to exacerbate splaying (Figure 3, C-E; Supplemental Figure S1, C and F). For instance, when ablated k-fiber stubs in GW108X-treated cells splay, they often remain splayed for longer, a phenomenon far less pronounced in cells treated with Kif15-IN-1 (Figure 3C). On average, these k-fiber stubs also undergo more cumulative splaying over the course of the entire spindle repair process, demonstrating that Kif15 crosslinking is instrumental in the maintenance and reformation of inter-microtubule bonds within ablated k-fiber stubs (Figure 3D). The appearance of this effect specifically following exposure to GW108X, but not KIF15-IN-1, suggests that the relevant function of Kif15, as it relates to k-fiber stub splaying, is its inter-microtubule crosslinking. Furthermore, the increased total splaying for GW108X-treated k-fiber stubs coincides with decreased poleward transport, as shown by tracking the kinetochore's poleward displacement over the same period, more explicitly suggesting the pronounced splaying results specifically from the loss of Kif15 crosslinking, independent of the effects of GW108X treatment on poleward transport (Figure 3E). We see this dependence of Kif15 crosslinking even in unsevered k-fibers. This is especially striking when GW108X-treated spindles sometimes shorten or collapse during imaging (Supplemental Figure S1D): when k-fibers occasionally buckle during collapse, it frequently induces splaying in the middle of these fibers, resulting in microtubule bundles that are apparently connected at both the centrosome and kinetochore, but are clearly unattached along much of their lengths (Figure 3Fii). While we sometimes see untreated spindle shorten somewhat over the course of imaging, their k-fibers do not typically splay when this occurs (Figure 3Fi). Stabilization of Kif15's microtubule-bound state appears to prevent this buckling and splaying, as this behavior was seen less frequently in control spindles and was never

observed in cells treated with Kif15-IN-1, which seems inline with the role of Kif15 in stabilizing kinetochore-microtubules during metaphase (Gayek and Ohi 2014).

Altogether, these data suggest that, in addition to contributing to outward spindle-axis force generation, Kif15 promotes the mechanical cohesion of k-fibers along their lengths by crosslinking microtubules to form and maintain tightly bound bundles. By doing so, Kif15 helps the k-fiber both maintain its structural integrity under duress and, when its characteristic structure has been compromised, efficiently reform into a cohesive parallel microtubule array (Figure 4). It will be interesting to determine the significance and nature of Kif15's functions in k-fiber structural maintenance and repair in other mammalian cell types in which the spindle itself faces additional mechanical challenges and constraints, such as crowding from higher numbers of chromosomes. Additionally, the physical responsibilities of other known microtubule crosslinkers, such as the clathrin/TACC3/ch-TOG complex and HURP, in promoting k-fiber structural integrity merits further investigation.

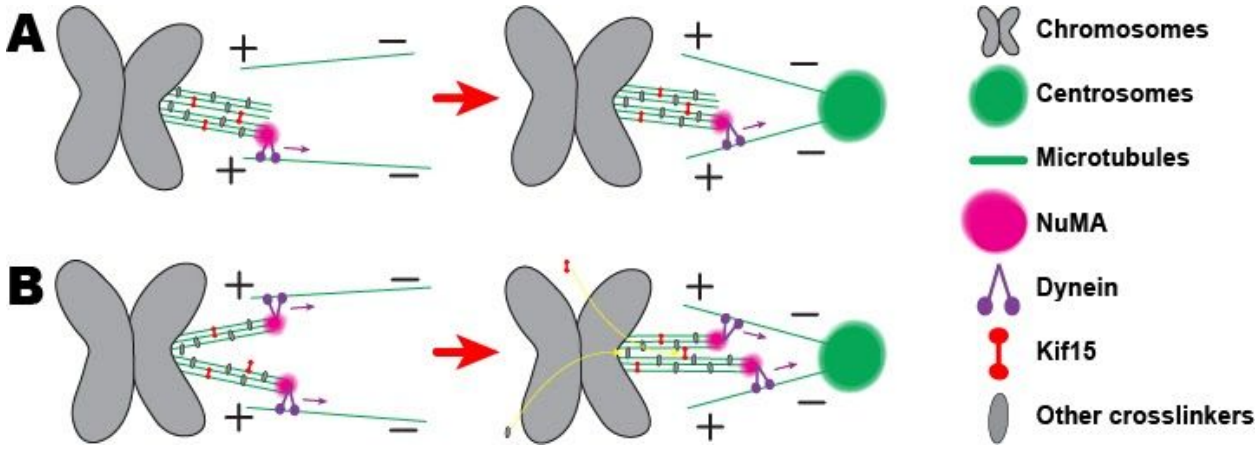

Figure 4: Kif15 crosslinking encourages the formation and maintenance of k-fiber microtubule cohesion. (A & B) During spindle repair, the microtubules of some k-fiber stubs remain tightly bound together, while others splay apart. (A) Microtubule pairs crosslinked by Kif15 often withstand spindle forces during poleward transport. (B) When k-fiber stubs splay, Kif15 re-crosslinks microtubules to "zip up" splayed k-fiber stubs. When Kif15 microtubule binding is perturbed, k-fiber stubs are more likely to splay even before, or in the absence of, poleward transport.

Materials & Methods

Cell culture

Wild type Ptk2 cells and Ptk2 stably expressing GFP-α-tubulin (both a gift of Sophie Dumont, UCSF) were cultured in MEM (Genesee 25-504 or Fisher 11095080) supplemented with non-essential amino acids (Genesee 25-536), sodium pyruvate (Genesee 25-537), penicillin/streptomycin (Genesee 25-512), and heat-inactivated fetal bovine serum (Genesee 25-514H). For live imaging, cells were plated in 9.6 cm^2 glass-bottom dishes treated with poly-D-lysine (MatTek P35GC-1.5-14-C) in 2 mL of MEM-complete (described above). For

immunofluorescence experiments, cells were plated on #1.5 25 mm coverslips (HCl cleaned and treated with poly-L-lysine) in a 6-well plate.

Drug treatment

For treatment with KIF15-IN-1 (Apex Bio), inhibitor was added to plated cells at a final concentration 12.5 μM (from stock in DMSO) and imaging was performed 1-2 hours after treatment. For treatment with GW108X (custom synthesis as previously described (Dumas et al. 2019)), inhibitor was added to plated cells at a final concentration 25 μM (from stock in DMSO) and imaging was performed within 1 hour of treatment. For treatment with S-trityl-L-cysteine (STLC) (Sigma-Aldrich 164739-5G), inhibitor was added to plated cells at a final concentration 5 μM (from stock in DMSO) and imaging was performed within 1 hour of treatment. Using these conditions, morphological signs of both KIF15-inhibition and Eg5-inhibition in spindles (such as shortened spindles) were detectable, but many spindles still displayed fairly normal overall bipolar morphology. Although monopoles and fully-collapsed bipoles were often observed, further verifying successful treatment, we did not perform ablation experiments on these cells.

Transfections & siRNA

For NuMA siRNA experiments, GFP-α-tubulin Ptk2 cells were transfected with siRNA for NuMA as previously described (Udy et al. 2015; Elting et al. 2017). The sequence for our siNuMA was 5'-GCATAAAGCGGAGACUAAA-3', designed based on the Ptk2 transcriptome, and Oligofectamine (Invitrogen 12252-011) was used for transfection reagent (Udy et al. 2015; Elting et al. 2017). Transfected plates were either fixed or imaged live 48-96 hr following treatment, with most experiments conducted on the third day after transfection. We verified our knockdown by observing NuMA expression and localization in fixed cells via immunofluorescence assays. In live cells, we also frequently observed spindle abnormalities, such as splayed or multiple poles, further verifying successful NuMA knockdown. However, we chose cells with bipolar spindles for ablation experiments, in order to focus on a direct effect of NuMA rather than effects of perturbing overall spindle architecture.

Immunofluorescence

Immunofluorescence was used to verify knockdown siRNA of NuMA. For fixation, cells were treated for three minutes with a solution of 95% methanol and 4.8mM EGTA. The following antibodies were used for these experiments: mouse anti-α-tubulin DM1α (1:500, Invitrogen 62204), rabbit anti-NuMA (1:400, Novus Biologicals NB500-174SS), human anti-centromere protein (CREST; 1:25, Antibodies Inc 15-234), fluorescent secondary antibodies (1:500, Invitrogen), and Hoechst 33342 (Invitrogen H3570). Coverslips were mounted on slides using Prolong Gold. Following fixation, cells were imaged using the confocal fluorescence microscope described below. For verifying knockdown, identical conditions (for fixation, staining, and imaging) were used to compare knockdown and control cells.

Live cell imaging and laser ablation

For live cell imaging, cells were plated in 9.6 cm^2 glass-bottom poly-D-lysine-coated dishes (MatTek P35GC-1.5-14-C) in 2mL of MEM-complete (described above) and left in an incubator at 37ºC and 5% CO_2 until time for imaging.

Live imaging and ablation experiments were performed essentially as previously described (Elting et al. 2017). In this case, live imaging was performed on a Nikon Ti-E stand on an Andor Dragonfly spinning disk confocal fluorescence microscope; spinning disk dichroic Chroma ZT405/488/561/640rpc; 488 nm (50 mW) diode laser (240 ms exposures) with Borealis attachment (Andor); emission filter Chroma Chroma ET525/50m; and an Andor iXon3 camera. Imaging was performed with a 100x 1.45 Ph3 Nikon objective and a 1.5x magnifier (built-in to the Dragonfly system). Frames were collected every 0.3-4.0 s for up to ~4 minutes after ablation. Targeted laser ablation was performed using an Andor Micropoint attachment with galvo-controlled steering to deliver 20-30 3 ns pulses at 20 Hz of 551 nm light. Andor Fusion software was used to control acquisition and Andor IQ software was used to simultaneously control the laser ablation system. For all experiments involving live cells, imaging was conducted on a closed stagetop incubator (Okolab), which maintains conditions of 30ºC, 5% CO_2 and humidity.

Data analysis

FIJI was used to prepare all videos for analysis. This process consisted of cropping frames, adjusting brightness and contrast, and converting file types. We cropped GFP-α-tubulin ablation images, in order to more clearly track the positions and splay angles of ablated k-fiber stubs. Videos were saved as both a TIFF stack and an AVI copy for each. The 'No Compression' option in FIJI was used, when saving videos as AVI files. Linear adjustments were made to the brightness and contrast of immunofluorescence, cotransfection, and GFP-α-tubulin ablation videos. The brightness and contrast of all videos in each immunofluorescence and cotransfection data were scaled the same as all other videos in the set.

In videos of GFP-α-tubulin spindles, spindle length was measured using the 'line' tool in FIJI. These measurements were conducted at the beginning of imaging of the spindle, to prevent potential effects on spindle length of long term imaging. Poles were identified as the center of high-intensity circles at the spindle ends. The focus of radial microtubule bundles was designated as the pole position for poles that were out of focus or dim.

Following ablations, k-fiber stubs first drifted away from the pole, toward the spindle midzone, before being transported poleward. When a k-fiber stub was not visibly transported poleward during at least four minutes of imaging, this was counted as an instance in which spindle repair (and poleward transport) does not transpire. We define poleward transport onset as the time at which the distance between the ablated k-fiber stub's kinetochore and pole is maximal. This was done via a tracking program, written in Python, for videos in which both the kinetochore and pole remain visible throughout. Poles were identified in a manner similar to that used to measure spindle length and kinetochore positions were defined as k-fiber stub plus-ends. Video playback was used, as many times as needed, to verify all pole and kinetochore position measurements.

Another tracking program, home written in Python, was used to measure ablated k-fiber stub splay angle. For videos in which the k-fiber stub was visible throughout, the splay angle was defined as the angle formed by the k-fiber stub's plus-end and the minus-ends of the two most separated splayed microtubule bundles. Occasionally, microtubule bundles were not approximately straight. In this case, instead of clicking on the bundle's minus-end, clicks were made somewhere along the bundle's length, so that the measured splay angle more accurately reflects the angle between the bundles proximal to the kinetochore. All splay angle measurements are verified by video playback, as many times as needed. Splay durations were measured as the length of uninterrupted time for which a k-fiber stub was splayed at an angle greater than 15°. Before applying this splay angle threshold, splay angle vs time data were smoothed using a 7-point binomial filter (Aubury and Luk 1996; Marchand and Marmet 1983); Figure 2, A and B; Figure 3C; Supplemental Figure S1E), making it easier to identify the initiation and conclusion of each splaying event. This same filter was applied to the k-fiber stub displacement vs. time data for calculating the instantaneous velocity (Figure 2, A and B).

Acknowledgments

We thank Sophie Dumont, Dick McIntosh, Christina Hueschen, Jon Kuhn, Alex Long, and Elting Lab members for helpful discussions about the work. We thank Sophie Dumont (UCSF) for the gift of Ptk2 cells expressing GFP-α-tubulin. We thank Eva Johannes and Mariusz Zareba of the North Carolina State University Cellular and Molecular Imaging Facility for helpful discussions and assistance with microscopy. MWE and MAB were supported by a Ralph E. Powe Junior Faculty Enhancement Award from the Oak Ridge Associated Universities. RO and ALS are supported by R01 GM086610. The authors declare no competing financial interests.

References

Aubury, Matthew, and Wayne Luk. 1996. "Binomial Filters." *Journal of VLSI Signal Processing Systems for Signal, Image, and Video Technology* 12 (1): 35–50.

Bird, Alexander W., and Anthony a. Hyman. 2008. "Building a Spindle of the Correct Length in Human Cells Requires the Interaction between TPX2 and Aurora A." *The Journal of Cell Biology* 182 (2): 289–300.

Booth, Daniel G., Fiona E. Hood, Ian A. Prior, and Stephen J. Royle. 2011. "A TACC3/ch-TOG/clathrin Complex Stabilises Kinetochore Fibres by Inter-Microtubule Bridging." *The EMBO Journal* 30 (5): 906–19.

Cheeseman, Liam P., Edward F. Harry, Andrew D. McAinsh, Ian A. Prior, and Stephen J. Royle. 2013. "Specific Removal of TACC3--Ch-TOG--Clathrin at Metaphase Deregulates Kinetochore Fiber Tension." *Journal of Cell Science* 126 (9): 2102–13.

Drechsler, Hauke, Toni McHugh, Martin R. Singleton, Nicholas J. Carter, and Andrew D. McAinsh. 2014. "The Kinesin-12 Kif15 Is a Processive Track-Switching Tetramer." *eLife* 3 (March): e01724.

Dumas, Megan E., Geng-Yuan Chen, Nicole D. Kendrick, George Xu, Scott D. Larsen, Somnath Jana, Alex G. Waterson, et al. 2019. "Dual Inhibition of Kif15 by Oxindole and Quinazolinedione Chemical Probes." *Bioorganic & Medicinal Chemistry Letters*.

https://doi.org/10.1016/j.bmcl.2018.12.008.
Elting, Mary Williard, Christina L. Hueschen, Dylan B. Udy, and Sophie Dumont. 2014. “Force on Spindle Microtubule Minus Ends Moves Chromosomes.” *The Journal of Cell Biology* 206 (2): 245–56.
Elting, Mary Williard, Manu Prakash, Dylan B. Udy, and Sophie Dumont. 2017. “Mapping Load-Bearing in the Mammalian Spindle Reveals Local Kinetochore Fiber Anchorage That Provides Mechanical Isolation and Redundancy.” *Current Biology: CB* 27 (14): 2112–22.e5.
Gaglio, T., A. Saredi, J. B. Bingham, M. J. Hasbani, S. R. Gill, T. A. Schroer, and D. A. Compton. 1996. “Opposing Motor Activities Are Required for the Organization of the Mammalian Mitotic Spindle Pole.” *The Journal of Cell Biology*. https://doi.org/10.1083/jcb.135.2.399.
Gayek, A. Sophia, and Ryoma Ohi. 2014. “Kinetochore-Microtubule Stability Governs the Metaphase Requirement for Eg5.” *Molecular Biology of the Cell* 25 (13): 2051–60.
Goshima, Gohta, François Nédélec, and Ronald D. Vale. 2005. “Mechanisms for Focusing Mitotic Spindle Poles by Minus End-Directed Motor Proteins.” *The Journal of Cell Biology* 171 (2): 229–40.
Hays, T. S., and E. D. Salmon. 1990. “Poleward Force at the Kinetochore in Metaphase Depends on the Number of Kinetochore Microtubules.” *The Journal of Cell Biology* 110 (2): 391–404.
Hays, T. S., D. Wise, and E. D. Salmon. 1982. “Traction Force on a Kinetochore at Metaphase Acts as a Linear Function of Kinetochore Fiber Length.” *The Journal of Cell Biology* 93 (2): 374–89.
Hueschen, Christina L., Samuel J. Kenny, Ke Xu, and Sophie Dumont. 2017. “NuMA Recruits Dynein Activity to Microtubule Minus-Ends at Mitosis.” *eLife* 6 (November). https://doi.org/10.7554/eLife.29328.
Kapitein, Lukas C., Erwin J. G. Peterman, Benjamin H. Kwok, Jeffrey H. Kim, Tarun M. Kapoor, and Christoph F. Schmidt. 2005. “The Bipolar Mitotic Kinesin Eg5 Moves on Both Microtubules That It Crosslinks.” *Nature* 435 (7038): 114–18.
Khodjakov, Alexey, Lily Copenagle, Michael B. Gordon, Duane A. Compton, and Tarun M. Kapoor. 2003. “Minus-End Capture of Preformed Kinetochore Fibers Contributes to Spindle Morphogenesis.” *The Journal of Cell Biology*. https://doi.org/10.1083/jcb.200208143.
Ma, Hoi Tang, Sergio Erdal, Shan Huang, and Randy Y. C. Poon. 2014. “Synergism between Inhibitors of Aurora A and KIF11 Overcomes KIF15-Dependent Drug Resistance.” *Molecular Oncology* 8 (8): 1404–18.
Mameren, Joost van, Karen C. Vermeulen, Fred Gittes, and Christoph F. Schmidt. 2009. “Leveraging Single Protein Polymers to Measure Flexural Rigidity.” *The Journal of Physical Chemistry. B* 113 (12): 3837–44.
Mann, Barbara J., Sai K. Balchand, and Patricia Wadsworth. 2017. “Regulation of Kif15 Localization and Motility by the C-Terminus of TPX2 and Microtubule Dynamics.” *Molecular Biology of the Cell*. https://doi.org/10.1091/mbc.e16-06-0476.
Marchand, P., and L. Marmet. 1983. “Binomial Smoothing Filter: A Way to Avoid Some Pitfalls of Least-squares Polynomial Smoothing.” *The Review of Scientific Instruments* 54 (8): 1034–41.
Mayr, Monika I., Stefan Hümmer, Jenny Bormann, Tamara Grüner, Sarah Adio, Guenther Woehlke, and Thomas U. Mayer. 2007. “The Human Kinesin Kif18A Is a Motile Microtubule Depolymerase Essential for Chromosome Congression.” *Current Biology: CB* 17 (6): 488–98.
McDonald, K. L., E. T. O’Toole, D. N. Mastronarde, and J. R. McIntosh. 1992. “Kinetochore

Microtubules in PTK Cells." *The Journal of Cell Biology* 118 (2): 369–83.
McHugh, Toni, Hauke Drechsler, Andrew D. McAinsh, Nicolas J. Carter, and Robert A. Cross. 2018. "Kif15 Functions as an Active Mechanical Ratchet." *Molecular Biology of the Cell* 29 (13): 1743–52.
Milic, Bojan, Anirban Chakraborty, Kyuho Han, Michael C. Bassik, and Steven M. Block. 2018. "KIF15 Nanomechanics and Kinesin Inhibitors, with Implications for Cancer Chemotherapeutics." *Proceedings of the National Academy of Sciences of the United States of America* 115 (20): E4613–22.
Mitchison, T. J. 1989. "Polewards Microtubule Flux in the Mitotic Spindle: Evidence from Photoactivation of Fluorescence." *The Journal of Cell Biology* 109 (2): 637–52.
Nicklas, R. B., D. F. Kubai, and T. S. Hays. 1982. "Spindle Microtubules and Their Mechanical Associations after Micromanipulation in Anaphase." *The Journal of Cell Biology* 95 (1): 91–104.
Nixon, Faye M., Cristina Gutiérrez-Caballero, Fiona E. Hood, Daniel G. Booth, Ian A. Prior, and Stephen J. Royle. 2015. "The Mesh Is a Network of Microtubule Connectors That Stabilizes Individual Kinetochore Fibers of the Mitotic Spindle." *eLife* 4 (JUNE2015): 1–21.
Qiao, Yuan, Jingtao Chen, Chao Ma, Yingmin Liu, Peitong Li, Yalin Wang, Lin Hou, and Ziling Liu. 2018. "Increased KIF15 Expression Predicts a Poor Prognosis in Patients with Lung Adenocarcinoma." *Cellular Physiology and Biochemistry: International Journal of Experimental Cellular Physiology, Biochemistry, and Pharmacology* 51 (1): 1–10.
Raaijmakers, Jonne a., Roy G. H. P. van Heesbeen, Johnathan L. Meaders, Erica F. Geers, Belen Fernandez-Garcia, René H. Medema, and Marvin E. Tanenbaum. 2012. "Nuclear Envelope-Associated Dynein Drives Prophase Centrosome Separation and Enables Eg5-Independent Bipolar Spindle Formation." *The EMBO Journal* 31 (21): 4179–90.
Rath, Oliver, and Frank Kozielski. 2012. "Kinesins and Cancer." *Nature Reviews. Cancer* 12 (8): 527–39.
Reinemann, Dana N., Emma G. Sturgill, Dibyendu Kumar Das, Miriam Steiner Degen, Zsuzsanna Vörös, Wonmuk Hwang, Ryoma Ohi, and Matthew J. Lang. 2017. "Collective Force Regulation in Anti-Parallel Microtubule Gliding by Dimeric Kif15 Kinesin Motors." *Current Biology: CB* 27 (18): 2810–20.e6.
Royle, Stephen J., Nicholas A. Bright, and Leon Lagnado. 2005. "Clathrin Is Required for the Function of the Mitotic Spindle." *Nature* 434 (7037): 1152–57.
Silljé, Herman H. W., Susanna Nagel, Roman Körner, and Erich A. Nigg. 2006. "HURP Is a Ran-Importin β-Regulated Protein That Stabilizes Kinetochore Microtubules in the Vicinity of Chromosomes." *Current Biology: CB* 16 (8): 731–42.
Sturgill, Emma G., Dibyendu Kumar Das, Yoshimasa Takizawa, Yongdae Shin, Scott E. Collier, Melanie D. Ohi, Wonmuk Hwang, Matthew J. Lang, and Ryoma Ohi. 2014. "Kinesin-12 Kif15 Targets Kinetochore Fibers through an Intrinsic Two-Step Mechanism." *Current Biology: CB* 24 (19): 2307–13.
Sturgill, Emma G., and Ryoma Ohi. 2013. "Kinesin-12 Differentially Affects Spindle Assembly Depending on Its Microtubule Substrate." *Current Biology: CB* 23 (14): 1280–90.
Sun, Yue-Feng, Hong-Li Wu, Rui-Fang Shi, Lin Chen, and Chao Meng. 2020. "KIF15 Promotes Proliferation and Growth of Hepatocellular Carcinoma." *Analytical Cellular Pathology* 2020 (April): 6403012.
Tanenbaum, Marvin E., Libor Macůrek, Aniek Janssen, Erica F. Geers, Mónica Alvarez-Fernández, and René H. Medema. 2009. "Kif15 Cooperates with eg5 to Promote Bipolar Spindle Assembly." *Current Biology: CB* 19 (20): 1703–11.
Terribas, Ernest, Marco Fernández, Helena Mazuelas, Juana Fernández-Rodríguez, Josep

Biayna, Ignacio Blanco, Gabriela Bernal, et al. 2020. “KIF11 and KIF15 Mitotic Kinesins Are Potential Therapeutic Vulnerabilities for Malignant Peripheral Nerve Sheath Tumors.” *Neuro-Oncology Advances*, January. https://doi.org/10.1093/noajnl/vdz061.

Tsuchiya, K., H. Hayashi, M. Nishina, and M. Okumura. 2018. “Importin-β Targets HURP to Kinetochore-Fibers in Coordination with Ran-GTP in Human Mitotic Cells.” *bioRxiv*. https://www.biorxiv.org/content/10.1101/473538v1.abstract.

Udy, Dylan B., Mark Voorhies, Patricia P. Chan, Todd M. Lowe, and Sophie Dumont. 2015. “Draft De Novo Transcriptome of the Rat Kangaroo Potorous Tridactylus as a Tool for Cell Biology.” *PloS One* 10 (8): e0134738.

Vladimirou, Elina, Nunu Mchedlishvili, Ivana Gasic, Jonathan W. Armond, Catarina P. Samora, Patrick Meraldi, and Andrew D. McAinsh. 2013. “Nonautonomous Movement of Chromosomes in Mitosis.” *Developmental Cell* 27 (1): 60–71.

Wang, Jie, Xingjun Guo, Chencheng Xie, and Jianxin Jiang. 2017. “KIF15 Promotes Pancreatic Cancer Proliferation via the MEK–ERK Signalling Pathway.” *British Journal of Cancer* 117 (2): 245–55.

Ye, Fan, Lora Tan, Qiaoyun Yang, Yun Xia, Lih-Wen Deng, Maki Murata-Hori, and Yih-Cherng Liou. 2011. “HURP Regulates Chromosome Congression by Modulating Kinesin Kif18A Function.” *Current Biology: CB* 21 (18): 1584–91.

Yu, Xiaoyu, Xiaoyu He, L. M. Heindl, Xin Song, Jiayan Fan, and Renbing Jia. 2019. “KIF15 Plays a Role in Promoting the Tumorigenicity of Melanoma.” *Experimental Eye Research* 185 (August): 107598.

Zhai, Y., P. J. Kronebusch, and G. G. Borisy. 1995. “Kinetochore Microtubule Dynamics and the Metaphase-Anaphase Transition.” *The Journal of Cell Biology* 131 (3): 721–34.

Zhao, Hongda, Qiyu Bo, Zonglong Wu, Qinggang Liu, Yan Li, Ning Zhang, Hu Guo, and Benkang Shi. 2019. “KIF15 Promotes Bladder Cancer Proliferation via the MEK-ERK Signaling Pathway.” *Cancer Management and Research* 11 (February): 1857–68.

Supplemental Information

Supplemental Figures

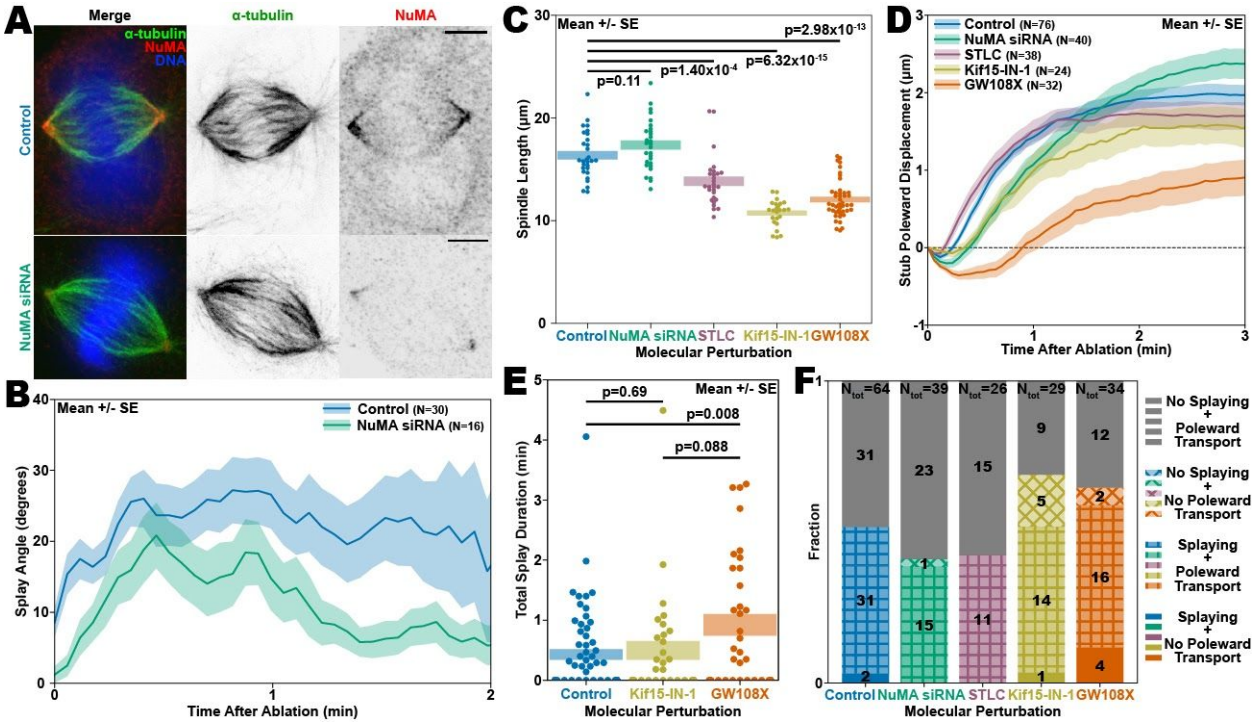

Supplemental Figure S1: (A) In immunofluorescence experiments, NuMA siRNA reduces NuMA k-fiber localization, particularly near the poles. All scalebars are 5 μm. While this example shows a bipolar spindle, typical of those that we use for ablation experiments, we also saw many spindles with splayed poles or multipolar spindles when we treated with siRNA for NuMA. (B) NuMA siRNA reduces splaying in splaying k-fiber stubs, compared with splaying k-fiber stubs in untreated cells. In contrast with Fig. 2E, this panel includes only splaying k-fiber stubs, and demonstrates that the effects in Fig. 2E are from a lower proportion of k-fiber stubs that splay combined with less splaying in those that do splay. Shaded regions represent average +/- standard error on the mean. (C) Eg5 and Kif15 inhibition results in shortened spindles. Shaded regions represent average +/- standard error on the mean and numbers at the top of the plot represent p-values. (D) NuMA siRNA and Kif15-IN-1 inhibition cause modest delays in poleward transport of ablated k-fiber stubs, while inhibiting Kif15 with GW108X results in poleward transport with severe delays and decreased overall magnitudes. Shaded regions represent average +/- standard error on the mean. (E) Kif15 inhibition with GW108X increases the time that k-fiber stubs remain splayed during repair. Shaded regions represent average +/- standard error on the mean and numbers at the top of the plot represent p-values. (F) Categorization of k-fiber stubs based on overall behavior. Numbers represent the number of k-fiber stubs exhibiting each behavior for each molecular condition and the total number of observed k-fiber stubs in each condition is given at the top of the corresponding bars. Note the number of Kif15-inhibited k-fiber stubs that do not undergo poleward transport (diagonal cross hatching and solid colors, yellow and orange), as well as those in GW108X-treated cells that are not reincorporated, but nonetheless splay (solid orange).

Supplemental Video Legends

Supplemental Video SV1. Typical example of an ablated k-fiber stub of a Ptk2 cell expressing GFP-α-tubulin which splays during poleward transport.

Supplemental Video SV2. Typical example of an ablated k-fiber stub of a Ptk2 cell expressing GFP-α-tubulin which does not splay during poleward transport.

Supplemental Video SV3. Typical example of an ablated spindle from a Ptk2 cell expressing GFP-α-tubulin and treated with GW108X. The ablated k-fiber stub splays before poleward transport, a behavior that is typical when treated with GW108X but very unusual in either cells treated with KIF15-IN-1 or in untreated control spindles.